

Electron transport in the dye sensitized nanocrystalline cell A Kambili^a, A B Walker^a, F Qiu^a, A C Fisher^b, A D Savin^b and L M Peter^b

^aDepartment of Physics, ^bDepartment of Chemistry, University of Bath, Bath BA2 7AY, UK

Abstract

Dye sensitised nanocrystalline solar cells (Grätzel cells) have achieved solar-to-electrical energy conversion efficiencies of 12% in diffuse daylight. The cell is based on a thin film of dye-sensitised nanocrystalline TiO₂ interpenetrated by a redox electrolyte. The high surface area of the TiO₂ and the spectral characteristics of the dye allow the device to harvest 46% of the solar energy flux. One of the puzzling features of dye-sensitised nano-crystalline solar cells is the slow electron transport in the titanium dioxide phase. The available experimental evidence as well as theoretical considerations suggest that the driving force for electron collection at the substrate contact arises primarily from the concentration gradient, ie the contribution of drift is negligible. The transport of electrons has been characterised by small amplitude pulse or intensity modulated illumination. Here, we show how the transport of electrons in the Grätzel cell can be described quantitatively using trap distributions obtained from a novel charge extraction method with a one-dimensional model based on solving the continuity equation for the electron density. For the first time in such a model, a back reaction with the I₃⁻ ions in the electrolyte that is second order in the electron density has been included.

PACS: 72.20.Jv,72.40+w,73.50.Pz,73.63Rt

Keywords: photovoltaics, nanocrystalline, transport.

1 Introduction

Dye-sensitised nanocrystalline cells were developed by Grätzel and coworkers [1, 2]. Their operation is shown in figure 1. Solar radiation is absorbed by a monolayer of a ruthenium based dye adsorbed on the surface of a porous nanocrystalline film consisting of electrically connected particles of \sim nm in diameter of TiO₂. On excitation of the dye by the radiation, electrons are transferred from the HOMO to the LUMO band of the dye, the latter lying just above the conduction band of the TiO₂, and then injected into the TiO₂ on timescales thought to be \sim fs [3, 4]. The TiO₂ film is permeated by an electrolyte which contains iodide ions (I⁻) and iodine in the form I₃⁻. The dye is regenerated by electron transfer from the I⁻ ions, leading to the formation of I₃⁻. In turn, the I₃⁻ ions are regenerated by electron transfer from the cathode, facilitated by a layer of platinum which acts as a catalyst. Electrons injected into the TiO₂ diffuse through the nanocrystalline film to the anode.

Whilst diffusion is slow in the electrolyte, the high concentrations of I₃⁻ and I⁻ ions result in loss free hole transport. Hence much of the research on these cells has focussed on electron transport in the nanocrystalline film since injected electrons are slowed down by trapping at the surface of the TiO₂ particles and may back react through

recombination with I₃⁻ ions. As the surface area/volume ratio is so high, it seems probable that traps at or near the surface dominate over those in the bulk. Back reaction with the dye ions occurs both through geminate reactions and from traps. It is likely that back reactions with the dye ions are reduced by efficient scavenging of the photo-generated holes by the I⁻ ions [2], so back reaction with I₃⁻ ions will be a significant cause of loss of efficiency. Measurements of the decay of the total electron concentration at open circuit show that the rate of back reaction with I₃⁻ ions is second order in the total electron concentration [5, 6], and possible back reaction sequences consistent with this observation were proposed in [7].

The response of the cell to time varying light intensities can yield much information about the density of traps, their energy distribution and the rate and nature of the back reaction. This can be done through the large amplitude measurements of electron decay in [5, 6], but these have the disadvantage that the whole trap distribution is sampled in a single measurement. More information can be obtained by employing intensity modulated photocurrent spectroscopy (IMPS) and intensity modulated photovoltage spectroscopy (IMVS) which involve superimposing a small modulated component of light intensity on a dc component I_0 [2, 8]. A plot of the imaginary part of the modulated photocurrent against the real part of the same quantity gives a semicircle in the negative imaginary half of the Argand diagram. The imaginary component is negative as the response lags behind the light intensity and is the majority carrier [2]. The magnitude of the imaginary response is a maximum when the cell is being perturbed at a frequency ω_{min} which is the inverse of its response time τ . Here, τ is the mean transit time for electrons through the TiO₂ network, allowing for electron scattering which is included in the bare diffusion coefficient D_{bare} (ie without traps), and multiple trapping. A similar result can be derived for the photovoltage.

We have used this approach to find how τ from IMPS spectra varies with the background intensity I_0 . Increasing I_0 results in an increase in the conduction band density and hence the electron quasi-Fermi level E_{Fn} . As E_{Fn} resides in the bandgap, changing I_0 scans E_{Fn} through the trap levels. Given that the response is dominated by states near E_{Fn} , IMPS and IMVS provide a means of probing the trap density of states. This was shown [9] for a first order backreaction with the assumption that the gradient of the electron quasi-Fermi level is constant.

Below, we show how ω_{min} can be calculated from a multiple trapping model in which electron transport is mediated by the conduction band and is interrupted by trapping. An alternative approach is the hopping model in which it is assumed that the electrons are always in a trapped state and transport is achieved by hopping from one trap to another. Recently, Nelson et al [10] looked at both models using a random walk Monte Carlo model utilising the continuous time random walk method of Scher and Montroll [11] where steps to all nearest neighbours are equally likely and the waiting time depends only on the energy of the initial site, and which included the back re-

action with I_3^- ions. They showed that the multiple trapping model is more capable than the hopping model of explaining experimental data on charge decay due to recombination.

To calculate the IMPS spectra, we solved the continuity equations for the conduction electron density and trapping probability. Our approach is a generalisation of that of Vanmaekelbergh and de Jongh [9] where we have included back reactions of first and second order and avoided the assumption that the gradient of the electron quasi-Fermi level is constant.

A common treatment of the transient response, used in [12], is to include the traps through an effective diffusion coefficient which depends on the conduction electron density or equivalently light intensity. For the diffusion coefficient D_{bare} we have taken the value measured on nanocrystalline anatase TiO_2 which has a small defect concentration. This is because we have explicitly allowed for the influence of electrolyte and defects in our model so they should not be also included in the diffusion coefficient. In [8], expressions for an effective diffusion coefficient and effective transition time that explicitly show the influence of the traps and back reaction were obtained from a similar model to ours but for a single trap level and a first order back reaction. However, in our model the physical meaning of these quantities is not clear.

2 Method

The rate of change of electron density $n(x, t)$, where x is the distance from the anode and t the time, is determined from the continuity equation for conduction electrons:

$$\frac{\partial n}{\partial t} = D_{bare} \frac{\partial^2 n}{\partial x^2} + \alpha I_0 \exp(-\alpha x) - k_{cb\mu}(n^\mu - n_{dark}^\mu) + \langle k_{detrap} N_{t0} f - k_{trap} n(1 - f) \rangle \quad (1)$$

Here the first term on the rhs is the photocurrent due to with diffusion coefficient without traps D_{bare} , the second term is the generation rate from light of intensity I_0 with an absorption coefficient α , the third term is the back reaction rate for conduction electrons with the I_3^- ions at a rate of $k_{cb\mu}$, where $\mu = 1$ for 1st order recombination, $\mu = 2$ for 2nd order recombination and n_{dark} the conduction electron density in the dark, and the fourth term is the net trapping rate whose terms are defined below. Equation 1 is coupled with the continuity equation for trapped electrons.

$$N_{t0} \langle \frac{\partial f}{\partial t} \rangle = \langle k_{trap} n(1 - f) - k_{detrap} N_{t0} f - k_{tb\mu}(n_{trap}^\mu - n_{trapdark}^\mu) \rangle \quad (2)$$

where N_{t0} is the density of traps, f the probability that a trap level is occupied, k_{trap} the trapping rate, k_{detrap} the detrapping rate and $k_{tb\mu}$ the back reaction rate for trapped electrons with the I_3^- ions. The angled brackets $\langle \rangle$ represent an average over the trap distribution, for any quantity A :

$$\langle A \rangle \equiv \int_{-E_g}^0 A(E_T) s(E_T) dE_T \quad (3)$$

where $s(E_T)dE_T$ is the probability of a trap site existing in the energy range $[E_T, E_T+dE_T]$ in the bandgap E_g , and is normalised so that it integrates to unity over the bandgap. Thus, the trapped electron density

$$n_{trap} = N_{t0} \langle f \rangle, \quad (4)$$

and $n_{trapdark}$ is n_{trap} in the dark. Detrapping by thermal excitation is assumed, so

$$k_{detrap} = \frac{k_{trap} N_c}{N_{t0}} \exp\left\{ \frac{E_T}{k_B T} \right\}, \quad (5)$$

where k_B is the Boltzmann constant.

An exponential trap distribution was used here in common with other authors ([10, 13]), using the parameter β to represent the width of the distribution in units of the thermal energy $k_B T$:

$$s(E_T) = \frac{\beta}{k_B T} \exp\left[\frac{\beta E_T}{k_B T} \right] \quad (6)$$

If β is large, say 0.3, most of the traps sit up near the conduction band, so detrapping will take place on average relatively quickly. As β is reduced, the probability of having deeper trap levels increases corresponding to longer detrapping times. The limits $\beta \rightarrow \infty$ and $\beta \rightarrow 0$ correspond respectively to all traps situated just below the conduction band and to a uniform trap distribution throughout the bandgap. We have also looked at Gaussian distributions as recent transient current measurements [14] suggest that the trap distribution may be peaked but these results will be published separately [15].

The photocurrent density

$$j_{photo}(x) = q D_{bare} \frac{\partial n}{\partial x} \quad (7)$$

where q is the magnitude of the electron charge. At the anode,

$$j_{photo}(0) = q k_{ext}(n(0) - n_{dark}), \quad (8)$$

where $k_{ext} = \sqrt{k_B T / (2m_n^* \pi)}$ for IMPS spectra (short circuit) and $k_{ext} = 0$ for IMVS spectra (open circuit). This is the Schottky boundary condition [16] with a recombination velocity $v_r = k_{ext}$. At the cathode side of the TiO_2 network,

$$j_{photo}(d) = 0. \quad (9)$$

The incident photon to electron conversion efficiency IPCE is $j_{photoss}(x=0)/qI_0$ where $j_{photoss}$ is the steady state photocurrent density. If trapping effects are neglected, it can be shown from equation 1 that the IPCE is equal to $1 - \exp(-\alpha d)$. The ac photocurrent conversion efficiency is $\Phi(\omega) = j_{photo}(x=0)/q\delta I_0$. We solved equations 1 and 2 in the steady state and for the modulated intensity $\delta I_0 \exp(i\omega t)$ (where $\delta I_0 \sim 0.01 I_0$ so that only the term linear in δI was included). Hence $\Phi(\omega)$ is complex.

As the electrostatic potential is screened out, classical statistics gives

$$n = N_c \exp(E_{Fn}/k_B T) \quad (10)$$

Table 1: Parameter values

Symbol	Value
D_{bare}	$1.0 \times 10^{-6} \text{ m}^2\text{s}^{-1}$
m_n^*	$9m_0$
N_c	$6.775 \times 10^{26} \text{ m}^{-3}$
α	$2.3 \times 10^5 \text{ m}^{-1}$
T	300 K
E_{Fndark}	-1.0 eV
k_{trap}	$1.0 \times 10^7 \text{ s}^{-1}$
d	$6 \times 10^{-6} \text{ m}$
$k_{cb2} = k_{tb2}$	$2 \times 10^{-25} \text{ m}^3\text{s}^{-1}$
β	0.2

where the conduction band density of states

$$N_c = 2 \left[\frac{m_n^* k_B T}{2\pi\hbar^2} \right]^{3/2} \quad (11)$$

where m_n^* is the effective mass and \hbar is Planck's constant divided by 2π .

To solve the equations, a relaxation method for a two point boundary value problem [17] was adopted. Second order kinetics resulted in nonlinear functional equations for the steady state and modulated components of f , which were solved using the Newton-Raphson method [17].

The parameter values are given in Table 1. D_{bare} and m_n^* (in units of the bare electron mass m_0) were taken from ref [18]. We deduced α by assuming an IPCE of 0.75 [19]. Our dark Fermi level E_{Fndark} comes from an estimate of 10^{11} m^{-3} for n_{dark} [7]. For an estimate for k_{trap} , we assumed that the trap cross-section σ would be in the region of $2 \times 10^{-22} \text{ m}^{-2}$, and that $k_{trap} = N_{t0} \sigma v_{th}$ where the thermal velocity of the electrons $v_{th} = \sqrt{2\pi} v_r$, but to keep the model simple, we made k_{trap} independent of N_{t0} . Our chosen values for k_{cb2}, k_{tb2} and β are discussed at the beginning of section 3.

3 Results

Our results are shown for a limited range of values of the trap density N_{t0} , trap distribution width β and back reaction rate k_{tb2} . We have set $k_{tb2} = k_{cb2}$ on the grounds of simplicity. Our results are insensitive to k_{cb2} as most of the electrons are trapped. We have chosen a value for k_{tb2} 100 times less than the value deduced from experiment [6] as this value was found to give better agreement between our IMPS predictions and experimental results.

For the parameter values shown, our calculations of ω_{min} give the best agreement with experiment for a range of values. How our predicted spectra vary with β and k_{tb2} will be presented in a separate paper [15], where our results for the IPCE as a function of intensity will also be given. We have not attempted to find a set of values of N_{t0}, k_{tb2} and β to give the closest fit to experimental data as the model does not seem accurate enough to justify this, and it is more instructive to see the trends in ω_{min} as N_{t0}, k_{tb2} and β are varied. We chose the values of

Table 2: Values $n(x=0)$ at different background intensities I_0 ($\text{m}^{-2}\text{s}^{-1}$) and trap densities N_{t0} (m^{-3})

N_{t0}	$I_0 = 1 \times 10^{15}$	$I_0 = 1 \times 10^{19}$
2.3×10^{23}	9.41×10^{10}	8.35×10^{14}
2.3×10^{24}	8.53×10^{10}	8.34×10^{14}

N_{t0} from noting that the density of states obtained from charge extraction measurements [5] is consistent with an exponential distribution of the type given in equation 6 for which $N_{t0} = 2.3 \times 10^{24} \text{ m}^{-3}$ and $\beta = 0.14$ [20]. However, more recent data suggests that β may be as high as 0.25 [21]. Our chosen value for β lies within this range, and it is at the bottom of the range of values suggested by Nelson et al [10] when modelling the decay of photoinduced dye cations.

3.1 Steady State Results

These results were obtained by setting the lhs of equations 1 and 2 to zero. In figure 2, we show an example profile for the conduction band density $n(x)$. This figure demonstrates the large density gradient that drives the electrons to the anode. The photocurrent is determined by the trap distribution at the anode where the electron density is much lower compared with its value on the cathode side. This means that there will be significant differences compared to IMVS spectra at the same intensity, for which $n(x)$ is almost constant throughout the TiO_2 film because of the boundary conditions forcing the gradient of $n(x)$ to be zero on both sides of the film. As the profiles for $n(x)$ are the same shape at all intensities and $n(x=0)$ is the only value needed for the photocurrent and IMPS results, we have only given our results for $n(x=0)$ which are shown in Table 2. These results show that $n(x=0)$ is nearly proportional to the light intensity, so that the IPCE is almost constant as would be expected for the low back reaction chosen. It is interesting to note that $n(x=0)$ is insensitive to the trap density at both light intensities.

The difference in behaviour for the different trap densities is rather seen in the steady state values for f at the anode which are shown in figure 3 for the same trap densities and light intensities as in Table 2. This graph shows the expected Fermi-Dirac distribution at the lower intensity, although for the lower trap density the spread in f is greater than for the higher trap density. This leads to a larger n_{trap} and hence back reaction rate compared to the solution for the higher trap density. From equation 2, setting the left hand side to zero in the steady state, it can be seen that a large back reaction forces f to be less than one at low trap energies, and this effect increases, the more n_{trap} exceeds $n_{trapdark}$. The same phenomenon is seen at the higher trap density but here the difference between n_{trap} and $n_{trapdark}$ is much greater at this density, forcing the observed low value of f at low trap energies.

The plateau between trap energies of -0.7 and -0.9 eV at the higher intensity and trap density resembles closely the plateaux predicted by Simmons and Taylor [22] in calculations of f in the steady state for bipolar semiconductors

with traps. Here, we have the same system except that it is unipolar and there is a second order back reaction, so the fact that we see the same features is reassuring. What is different from reference [22] is our result that f is less than unity even at trap levels deep into the conduction band. This is a direct consequence of the assumption that the back reaction rate is independent of the trap energy E_T , and may therefore be an artifact of the model. However, it does not unduly affect the results as what is important is the overlap with the trap distribution $s(E_T)$ and this decreases rapidly for low values of E_T .

3.2 IMPS Results

Figure 4 compares the predicted IMPS spectra for two light intensities. The spectrum is approximately semicircular. $\text{Im}(\Phi(\omega_{min}))$ at the higher intensity is about three times its value at the lower intensity. This can be qualitatively explained as being due to the greater losses due to the back reaction at the higher intensity.

The semicircle is a result of a single value for τ even though there is a distribution of trap levels; Vanmaekelbergh et al [9] note that this is a result of the capture rate for a given trap level varying inversely with the residence time. However at the higher intensity, where the back reaction is more important, the semicircle is more distorted as seen from figure 3. This distortion suggests that there is a dispersion in the electron arrival times at the anode [9]. For each spectrum, it can be seen that there is a single value of ω_{min} within the range of frequencies calculated. Whilst another value exists at much higher frequencies, this has not been calculated as it would occur well outside the frequencies accessible to experiment.

Our main result is shown in figure 5 where our predictions for ω_{min} are compared with experimental data from [23]. The magnitude of $\omega_{min} = 1/\tau$ is determined by the time taken in trapping and detrapping processes. As I_0 increases, the traps fill up (see figure 3) so that detrapping occurs from the shallower trap levels at which it takes place faster from equation 5. From figure 5, it is clear that at any given intensity over the range considered, ω_{min} decreases as N_{t0} increases. This is because if there are more traps, the likelihood of an electron being trapped and then detrapped en route to the anode increases, slowing it down so increasing τ .

The good agreement with experiment is encouraging. In our calculations for all three trap densities, we have achieved the same gradient of approx 0.8 for $\log_{10}(\omega_{min})$ vs $\log_{10}(I_0)$ as in the experiments at the higher intensities. However, unlike our calculations, the experimental results flatten off at the lower intensities. This effect seen in our calculations for larger values of k_{tb2} , although in our calculations the flattening off exceeds that seen experimentally. The flattening occurs because the trap probability in the steady state f does not differ greatly from its dark value except at the higher intensities.

4 Conclusions

We have shown for the first time with a one-dimensional model including explicitly trapping and back reaction with I_3^- ions that the assumption of a back reaction which is second order in the electron density gives values of ω_{min} deduced from IMPS spectra which are in good agreement with experiment. Our model will be useful in obtaining quantitative information from intensity modulated spectra on the trap distribution and back reaction and hence establish how different methods of cell fabrication yield different conversion efficiencies. Many questions however remain unanswered, for example whether the same parameters will give equally good agreement with IMVS spectra and whether a suitable set of parameters could give good agreement with experiment if a first order back reaction were assumed.

References

- [1] B O'Regan and M Grätzel Nature **353** 737 (1991)
- [2] L M Peter and D Vanmaekelbergh Advances in Electrochemical Science and Engineering **6** Eds R C Alkire and D M Kolb (VCH Wiley, 1999)
- [3] J M Rehm, G L McLendon, Y Nagasawa, K Yoshihara, J Moser and M Grätzel J Phys Chem B **100** 9577 (1996)
- [4] J R Durrant, Y Tachibana, I Mercer, J E Moser, M Grätzel and D R Klug Z Phys Chem **212** 93 (1999)
- [5] N W Duffy, L M Peter, R M G Rajapakse and K G U Wijayantha Electrochem Comm **2** 658 (2000)
- [6] N W Duffy, L M Peter, R M G Rajapakse and K G U Wijayantha J Phys Chem B **104** 8916 (2000)
- [7] A C Fisher, L M Peter, E A Ponomarev, A B Walker and K G U Wijayantha J Phys Chem B **104** 949 (2000)
- [8] L Dloczik, O Ileperuma, I Lauermann, L M Peter, E A Ponomarev, G Redmond, N J Shaw and I Uhlendorf J Phys Chem B **101** 10281-9 (1997)
- [9] D Vanmaekelbergh and P E de Jongh Phys Rev B **61** 4699 (2000)
- [10] J Nelson, S A Haque, D R Klug and J R Durrant Phys Rev B **63** 205321 (2001)
- [11] H Sher and E W Montroll Phys Rev B **12** 2455 (1975)
- [12] G Schlichthörl, N G Park and A J Frank J Phys Chem B **103** 782 (1999)
- [13] J van de Lagemaat and A J Frank J Phys Chem B **104** 4292 (2000)

- [14] H Wang, J He, G Boschloo, H Lindstrom, A Hagfeldt and S Lindquist *J Phys Chem B* **105** 2529 (2001)
- [15] A B Walker, L M Peter and F Qiu, manuscript in preparation
- [16] S M Sze *Physics of Semiconductor Devices 2nd Edition* (New York: John Wiley and Sons, 1981)
- [17] W H Press, S A Teukolsky, W T Vetterling and B P Flannery *Numerical Recipes in Fortran 2nd Edition* (Cambridge: Cambridge University Press, 1992)
- [18] B Enright and D Fitzmaurice *J Phys Chem* **100** 1027 (1996)
- [19] G Franco, J Gehring, L M Peter, E A Ponomarev and I Uhlendorf *J Phys Chem B* **103** 692 (1999)
- [20] A B Walker, unpublished work (2001)
- [21] N W Duffy and L M Peter, unpublished results (2001)
- [22] J G Simmons and G W Taylor *Phys Rev B* **4** 502 (1971)
- [23] L M Peter and K G U Wijayantha *Electrochem Comm* **1** 576 (1999)

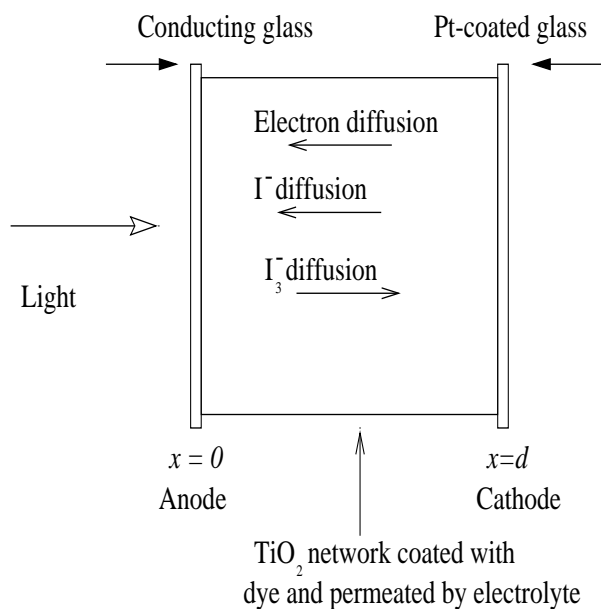


Figure 1: Schematic diagram of solar cell

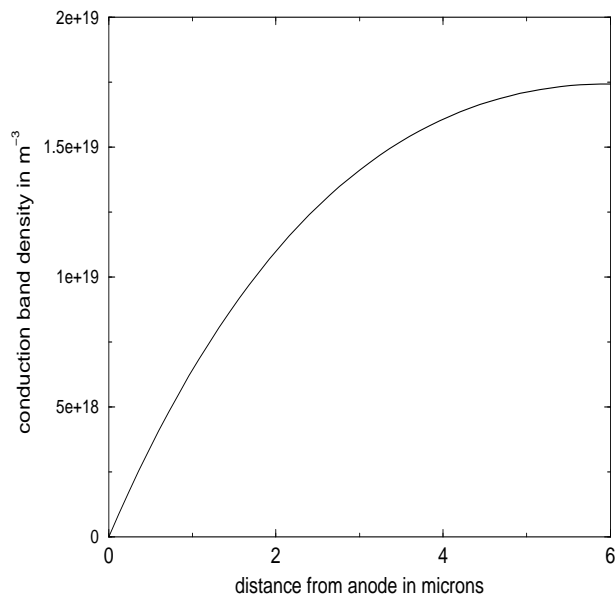


Figure 2: Conduction band density profile $n(x)$ where x is the distance from the anode for an intensity I_0 of $1 \times 10^{19} \text{m}^{-2} \text{s}^{-1}$ and a trap density N_{t0} of $2.3 \times 10^{24} \text{m}^{-3}$

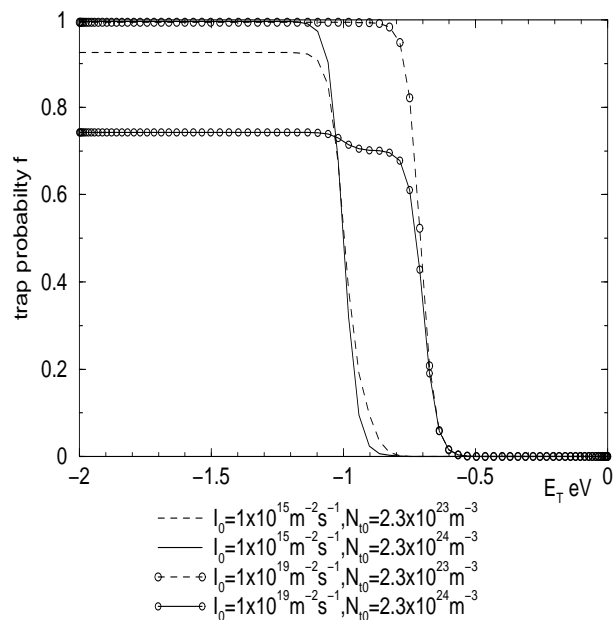


Figure 3: Trap occupation probability f as a function of the trap energy relative to the conduction band energy E_T for intensities I_0 of $1 \times 10^{15} \text{m}^{-2} \text{s}^{-1}$ and $1 \times 10^{19} \text{m}^{-2} \text{s}^{-1}$ and trap densities N_{t0} of $2.3 \times 10^{23} \text{m}^{-3}$ and $2.3 \times 10^{24} \text{m}^{-3}$

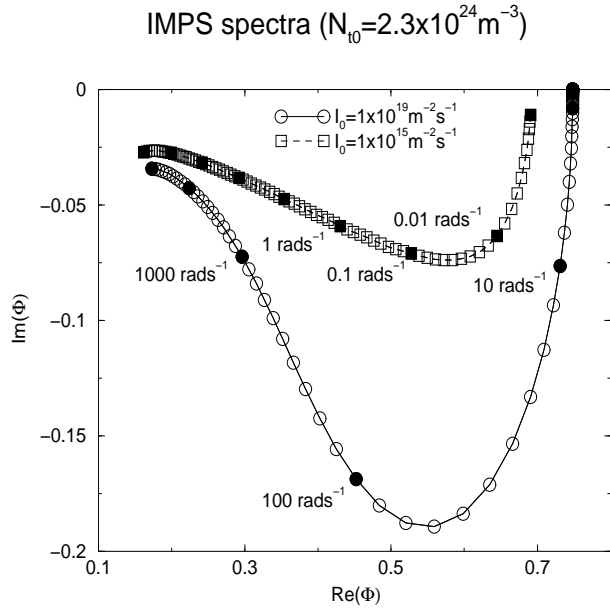


Figure 4: Imaginary part vs real part of the ac photocurrent conversion efficiency Φ at intensities I_0 of $1 \times 10^{15} \text{ m}^{-2} \text{ s}^{-1}$ (squares) and $1 \times 10^{19} \text{ m}^{-2} \text{ s}^{-1}$ and a trap density N_{t0} of $2.3 \times 10^{24} \text{ m}^{-3}$ (circles)

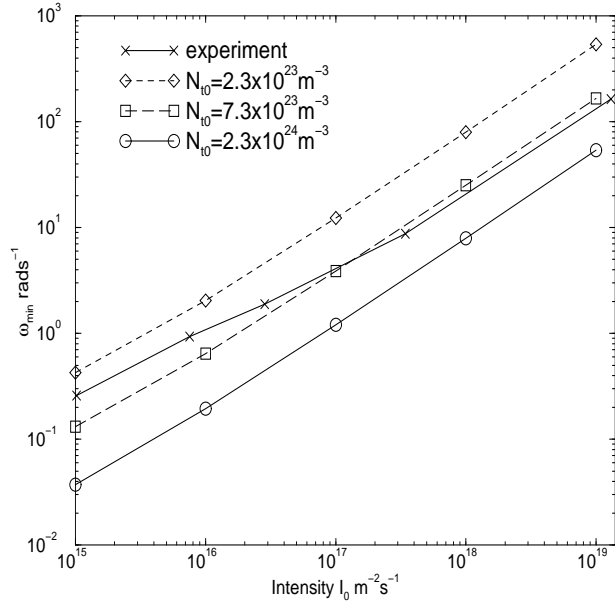


Figure 5: Minimum frequency ω_{min} vs background intensity I_0 for trap densities N_{t0} of $2.3 \times 10^{23} \text{ m}^{-3}$ (diamonds), $7.3 \times 10^{23} \text{ m}^{-3}$ (squares) and $2.3 \times 10^{24} \text{ m}^{-3}$ (circles) compared with experiment (crosses)